Published in final edited form as:
J Control Release. 2017 August 10; 259: 128–135. doi:10.1016/j.jconrel.2017.03.006.

PBCA-based Polymeric Microbubbles for Molecular Imaging and Drug Delivery

Patrick Koczera[#a,b], **Lia Appold**[#a], **Yang Shi**[a], **Mengjiao Liu**[a], **Anshuman Dasgupta**[a], **Vertika Pathak**[a], **Tarun Ojha**[a], **Stanley Fokong**[a], **Zhuojun Wu**[c], **Marc van Zandvoort**[c,d], **Olga Iranzo**[e], **Alexander Kuehne**[f], **Andrij Pich**[f], **Fabian Kiessling**[a,#], and **Twan Lammers**[a,g,h,#]

[a]Department of Experimental Molecular Imaging (ExMI), Helmholtz Institute for Biomedical Engineering, University Hospital RWTH, Pauwelsstr. 30, 52074 Aachen, Germany [b]Department of Intensive Care, University Hospital RWTH Aachen, Pauwelsstr. 30, 52074 Aachen, Germany [c]Institute for Molecular Cardiovascular Research, University Hospital RWTH Aachen, Pauwelsstr. 30, 52074 Aachen, Germany [d]Department of Genetics and Cell Biology - Molecular Cell Biology, Cardiovascular Research Institute Maastricht, Maastricht University Medical Centre, 6229 HX Maastricht, The Netherlands [e]Institute of Molecular Science, Aix Marseille University, UMR CNRS 7313, 13397 Marseille, France [f]DWI–Leibniz Institute for Interactive Materials, RWTH Aachen University, Forckenbeckstr. 50, 52056 Aachen, Germany [g]Department of Targeted Therapeutics, Institute for Biomedical Technology and Technical Medicine, University of Twente, PO Box 217, 7500 AE Enschede, The Netherlands [h]Department of Pharmaceutics, Utrecht Institute for Pharmaceutical Sciences, Utrecht University, Universiteitsweg 99, 3583 CG Utrecht, The Netherlands

[#] These authors contributed equally to this work.

Abstract

Microbubbles (MB) are routinely used as contrast agents for ultrasound (US) imaging. We describe different types of targeted and drug-loaded poly(n-butyl cyanoacrylate) (PBCA) MB, and demonstrate their suitability for multiple biomedical applications, including molecular US imaging and US-mediated drug delivery. Molecular imaging of angiogenic tumor blood vessels and inflamed atherosclerotic endothelium is performed by modifying the surface of PBCA MB with peptides and antibodies recognizing E-selectin and VCAM-1. Stable and inertial cavitation of PBCA MB enables sonoporation and permeabilization of blood vessels in tumors and in the brain, which can be employed for direct and indirect drug delivery. Direct drug delivery is based on US-induced release of (model) drug molecules from the MB shell. Indirect drug delivery refers to US- and MB-mediated enhancement of extravasation and penetration of co-administered drugs and drug delivery systems. These findings are in line with recently reported pioneering proof-of-principle studies showing the usefulness of (phospholipid) MB for molecular US imaging and sonoporation-enhanced drug delivery in patients. They aim to exemplify the potential and the broad applicability of combining MB with US to improve disease diagnosis and therapy.

[#]Corresponding author: tlammers@ukaachen.de.

Europe PMC Funders Author Manuscripts

Europe PMC Funders Author Manuscripts

1 Introduction

Ultrasound (US) imaging is, besides X-ray radiography, the most widespread clinical imaging modality. It combines the advantages of bedside availability and real-time imaging with cost- and time-effectiveness [1]. MB in the range of 1-10 μm, which consist of a gas- or air-filled core stabilized by a lipid- or polymer-based shell, are routinely used as contrast agents for US imaging. In general, imaging of soft-shell lipid-based MB is done using non-destructive US and it is based on their non-linear oscillation upon exposure to low- to medium-intensity US pulses (stable cavitation); on the other hand, destructive pulses (inertial cavitation) and backscattering – which becomes more important at higher US frequencies – are more frequently employed in case of hard-shell polymer-based MB [2–4].

Due to their size, which is too large for extravasation, MB can only be employed as intravascular contrast agents, allowing e.g. for the assessment of the perfusion of small vessels, which cannot be properly visualized using contrast agent-free (e.g. Power-Doppler-based) US imaging [5]. This is used in clinical practice for diagnosis, staging and functional characterization of e.g. cardiovascular and hepatic pathologies [6, 7]. Additionally, it can be used to characterize potential cancerous lesions, as angiogenesis is an important step in the transformation to malignancies, and as MB-based functional and molecular US imaging allow for accurate profiling, staging and treatment monitoring [6–8]. In such setups, the functional aspect of vessel imaging is restricted to the visualization and quantification of blood flow and flow velocity, while at the molecular level, information can be obtained on the (over-) expression of surface receptors, aiding in the more detailed characterization of tumor angiogenesis [11]. Among the surface receptors routinely used in molecular US imaging are classic angiogenic targets, like the vascular endothelial growth factor receptor 2 (VEGFR-2) and $\alpha_v\beta_3$ integrins, as well as inflammatory markers, such as the intercellular or vascular cell adhesion molecules ICAM and VCAM, and E- and P-selectins [10–14].

Besides for imaging, MB can also be used for drug delivery. The combination of MB and US can – via sonoporation and sonopermeabilization mechanisms – affect the integrity of the vascular lining and of cellular membranes [15–18]. This temporary perforation and the enhanced endo/transcytosis induced by stable and/or inertial MB cavitation is highly useful for temporally and spatially guiding drug delivery, e.g. to solid tumors or across the blood-brain barrier (BBB) [19–23]. The exact mechanisms contributing to enhanced drug delivery upon sonoporation are incompletely understood, as are differences in the sonoporation-potential of soft- vs. hard-shell MB, and targeted vs. untargeted MB [24, 25]. When exposed to US, MB rapidly shrink and swell, in line with the applied US frequency, and this results in physical effects such as microstreaming, microjets, ultrasonic shockwaves and MB compression/rarefaction-induced disruption of endothelial linings and cellular membranes [15–18, 26, 27]. These phenomena can contribute to enhanced extravasation, penetration and cellular uptake of drugs and drug delivery systems [20, 21, 28–30].

MB-mediated drug delivery can be subdivided into indirect and direct drug delivery. In case of the former, drugs or drug delivery systems are co-administered with MB and US. In case of direct drug delivery, drug molecules are embedded within the MB shell (or bound, in the form of drug delivery systems, to their surface) and locally released at the pathological site

in a temporally and spatially controllable manner [31–33]. Such externally triggerable drug targeting concepts are increasingly employed, also in patients, as exemplified e.g. by efforts to combine US-mediated hyperthermia with temperature-sensitive liposomes in liver cancer [34–37], as well as by recently published pioneering advances showing that sonoporation can be favorably employed in patients with pancreatic cancer and glioblastoma [38, 39].

With regard to direct drug delivery, one could argue that polymeric MB, because of their much thicker shell (50-150 nm), are advantageous as compared to lipid-based MB (3-5 nm), providing more space for drug loading [40, 41]. Polymeric MB might also allow for more diverse (and tailorable) modes of surface functionalization, via direct and indirect coupling mechanisms. In this manuscript, we exemplify the broad applicability of prototypic poly(n-butyl cyanoacrylate) (PBCA)-based MB for molecular US imaging and drug delivery applications. We extend previously published concepts for targeted US imaging of atherosclerosis and tumor angiogenesis, and for direct and indirect US-mediated drug delivery to tumors and to the brain. These findings exemplify the usefulness of combining MB with US for more efficient disease diagnosis and therapy.

2 Materials and methods

2.1 Synthesis of PBCA-based polymeric microbubbles

PBCA MB were synthesized by adding 3 ml of n-butyl cyanoacrylate (BCA, Special Polymers, Sofia, Bulgaria) dropwise to 300 ml of an aqueous solution containing 1% of Triton X-100 (Sigma Aldrich, Munich, Germany) at pH 2.5. The solution was stirred for 1 h at 10000 rpm and room temperature, and a suspension of air-filled polydispersed MB was obtained. MB with defined sizes were separated using multiple centrifugation and flotation steps. Additional washing steps were performed to purify the MB dispersion. MB size and concentration were measured with a Beckman Coulter Multisizer 3. Electron microscopy was performed using a Hitachi S4800 FESEM for scanning electron microscopy (SEM) with a Cryo-Gatan unit Alto 2500 at 1 kV and 2 μA. A drop of the aqueous MB suspension was placed on the sample holder and frozen using liquid nitrogen, before insertion into the preparation chamber. A Philips EM400T was used for transmission electron microscopy (TEM). The samples were fixed using 2 % agarose and dehydrated with ethanol before embedding in liquid epoxy resin. The resins were cut into 85 nm sections.

2.2 Drug loading into the shell of PBCA MB

The loading of (model) drug molecules into the shell of PBCA-based polymeric MB was performed via a one-step or two-step approach. Fluorescent dyes can be employed as model drugs, allowing for simple and straightforward quantification of loading and release, and facilitating *in vitro* and *in vivo* evaluation of cellular internalization and target site accumulation. In the one-step approach, 2.5 mg of rhodamine B (Applichem, Darmstadt, Germany) and/or coumarin 6 (Sigma Aldrich, Munich, Germany) were dissolved in 300 μl H_2O or dimethylformamide (DMF, Carl Roth, Karlsruhe, Germany), (respectively, for coumarin 6) and added at once before the BCA to the polymerization medium during the MB formation process. In the two-step approach, rhodamine B (2.5 mg in 200 μl H_2O), coumarin 6 (2.5 mg in 200 μl DMF) and/or the near infrared fluorophore 1,1',3,3,3',3'

hexamethyl-indotricarbocyanine-iodide (HITC, Sigma Aldrich, Munich, Germany) (10 mg in 100 μl DMSO (Carl Roth, Karlsruhe, Germany)) were post-loaded into the MB shell. Unloaded dye is removed from the MB-solution via several washing steps. MB are allowed to float and the solution underneath is refreshed until no free dye is left. After initially preparing a batch of size-optimized, surface-functionalized and/or actively targeted MB, the model drug solutions were added to 10 ml prepared MB under continuous stirring at room temperature. Measurements of fluorophore-loaded MB were performed using a Leica TCS SP8 X automated inverted confocal and stimulated emission depletion (STED) microscope equipped with a plan-apochromat 100 x/1.40 oil-immersion objective.

2.3 Surface functionalization and modification with targeting ligands

MB-shell functionalization was done via the EDC (i.e. N-(3-dimethylaminopropyl)-N-ethylcarbodiimide hydrochloride, Sigma Aldrich, Munich, Germany) coupling chemistry. The butyl-ester groups of the PBCA side-chains were partly hydrolyzed by increasing the pH to around 10 with NaOH (0.1 M, AppliChem, Darmstadt, Germany) for 15 minutes. The resulting carboxyl groups were activated by EDC (5×10^8 MB, 7.5 mg EDC) and streptavidin (300 μg, ChemImpex, Wood Dale, USA) or the E-selectin binding peptide IELLQAR (1 mg, Olga Iranzo, Marseille, France) were added to the MB suspension followed by stirring at 4 °C overnight. The functionalized MB were purified by several washing steps to remove the unreacted EDC and peptides and size-separated by centrifugation and flotation. Streptavidin-labeled MB (1×10^7) were further functionalized by coupling to biotinylated antibodies directed against VCAM-1 (5 μg, clone 429, eBioscience, Frankfurt, Germany) and VEGFR-2 (0.75 μg, Abcam, Cambridge, UK).

2.4 *Ex vivo* studies

All *in vivo* and *ex vivo* experiments were approved by institutional and governmental ethics boards. Fluorescent rhodamine B-loaded MB targeted against VCAM-1 via antibodies were used in 8-week-old male CD-1 wild-type mice. Endothelial activation (mimicking vascular inflammation) was achieved by intraperitoneal injection of recombinant murine TNF-α (PeproTech, Hamburg, Germany). Carotid arteries were excised 4 h after endothelial activation and mounted in a home-built flow-chamber. After 10 minutes of infusion with VCAM-1-targeted MB or unmodified control MB (diluted to a final concentration of 10^7 MB/ml in full blood; at a flow rate of 0.25 ml/min), carotid arteries were imaged *ex vivo* by two-photon laser scanning microscopy using an Olympus FV1000MPE multiphoton microscopy system (Mai Tai DeepSee pulsed Ti:Sapphire laser with 140 fs pulse width at an excitation wavelength of 800 nm) with a 25 x water dipping objective.

2.5 *In vivo* studies

To visualize and characterize tumor angiogenesis, E-selectin-targeted and non-targeted control MB (1×10^7 MB) were i.v. injected in CD1 nude mice bearing subcutaneous A431 human epidermoid cancer xenografts (ATCC CRL-1555; 6 mice per group). Replenishment analysis was used to distinguish between bound and unbound MB. US imaging was performed in the non-linear contrast mode using a VisualSonics Vevo2100 preclinical ultrasound system with a MS250 transducer operating at a frequency of 18 MHz of the tumor xenografts up until 7 minutes after i.v. injection. Before and after a destructive pulse,

the mean contrast intensity in the tumor region was compared. This was done after the replenishment phase, and allows for accurate monitoring of the expression of vascular markers, such as E-selectin. To test the ability of the PBCA MB for direct drug delivery purposes, mice with s.c. CT26 (ATCC CRL-2638) colon carcinoma allografts were injected with coumarin 6-loaded anti-VEGFR-2 antibody-targeted MB. MB were destroyed in the tumor vasculature by multiple destructive US pulses (non-linear contrast mode, Vevo2100, 18 MHz, MI = 1) at 7 minutes after MB injection, when the majority of the MB fraction in tumors corresponded to vessel-associated US contrast agents. Vessels were stained with i.v. injected rhodamine-labeled lectin at the end of the experiment, and tumor sections were used for histology to image MB-mediated delivery, accumulation and penetration of coumarin 6 in mice with CT26 using fluorescence microscopy.

We also evaluated indirect enhancement of drug delivery, via sonoporation of the BBB. This was done in healthy CD1 nude mice, using 8.5 x 10^8 USPIO-loaded MB i.v. (infused for 5 minutes into the tail vein) in combination with co-injected FITC-labeled dextran (70 kDa, Sigma Aldrich, Munich, Germany; 200 mg/kg in 0.9 % saline). Power Doppler US was performed for 5 minutes at a frequency of 16 MHz over the skull of mice compared to control animals, which only received MB without US. Tumors and brain tissue were harvested, mounted, frozen and cut using a Leica CM3050S cryostat. Tissue sections (8 μm) were analyzed using the Carl Zeiss AxioImager M2 microscopy system. Perfused blood vessels were stained using rhodamine-labeled lectin, enabling simultaneous microscopy imaging of the vasculature and of FITC-dextran extravasation and penetration.

3 Results and discussion

3.1 Preparation and functionalization of PBCA-based polymeric microbubbles

The synthesis of PBCA MB, and representative scanning and transmission electron microscopy images are shown in Figure 1A. Chemical modification of the shell of PBCA MB allows for functionalization of their surface, which facilitates specific binding of the MB (Figure 1B). After partial hydrolysis of the MB shell, surface functionalization was performed via EDC-coupling with streptavidin and subsequent use of biotinylated antibodies, as well as via direct EDC coupling of small oligomeric peptides (Figure 1C). The specificity of the targeted MB was initially tested *in vitro*. To this end, the binding of targeted MB to activated endothelial cells was compared, by means of fluorescent microscopy, to non-targeted MB as well as to targeted MB binding under blocking conditions [42, 43]. Results were confirmed *in vivo* (see below). Using such setups, multiple antibody-targeted PBCA-based MB have already been shown to hold potential for molecular US imaging [42, 44–46].

The straightforward synthesis of PBCA MB leads to MB dispersions with relatively broad size distribution. After 1-3 centrifugation/flotation rounds, a MB population with an acceptable size distribution and with a mean size of ~ 2 μm was isolated (Figure 2A). Optimized centrifugation/flotation protocols furthermore allow for the isolation of MB batches with varying size populations, i.e. 1, 2 and 3 μm in diameter (Figure 2D). Afterwards, hydrophilic and hydrophobic model drugs (i.e. rhodamine B, coumarin 6 and HITC) were loaded into the shell of PBCA MB (Figure 2B-C). Successful co-loading of

rhodamine B and coumarin 6 was also demonstrated (right panel in Figure 2C). Cryo-scanning electron microscopy was employed as a means to assess the shell-thickness of PBCA MB. In Figures 2F-G, MB were destroyed and cryogenically fixed, to visualize the outer and inner structure of the shell. In these SEM analyses, the shell-thickness appeared to be in the order of 50 nm. STED microscopy (of intact MB) on the other hand indicated a shell-thickness of 150-200 nm (Figure 2E). This difference in shell thickness likely results from the shrinkage of the MB shell during the freezing process required for cryo-SEM. It is anticipated that the results obtained using STED microscopy more accurately ß reflect the real shell thickness of PBCA MB.

These results exemplify the versatility of PBCA MB for targeting and shell loading, and they demonstrate that they can be easily synthesized and customized for purposes ranging from molecular imaging to drug delivery.

3.2 PBCA MB for molecular imaging in angiology

We developed VCAM-1-targeted MB by coupling anti-VCAM-1 antibodies to the shell of rhodamine B-loaded PBCA MB via biotin-streptavidin linkages. VCAM-1 is known to be overexpressed on endothelial cells affected by inflammatory stimuli, e.g. in case of atherosclerosis. This is schematically depicted in Figure 3A. In line with this, Figure 3B shows the *ex vivo* binding of VCAM-1-targeted PBCA MB to the inflamed endothelial lining of TNF-α-activated carotid arteries by 3D two-photon laser scanning microscopy (3D-TPLSM) in comparison to non-targeted MB. These *ex vivo* flow-chamber results are in line with the in vivo data previously reported by Curaj et al., who showed that VCAM-1-targeted MB are useful for longitudinally monitoring vascular healing after arterial injury [47]. They longitudinally examined carotid arteries of ApoE deficient mice under high fat diet *in vivo* and *ex vivo* by VCAM-1-targeted CEUS and 3D-TPLSM after wire-injury. The VCAM-1-specific PBCA MB showed accumulation at the injured site and variation of enhancement in the course of regeneration, with a peak after 3 days.

A related target for molecular US imaging of atherosclerosis is ICAM-1. In a similar flow-chamber setup, TNF-α induced arterial inflammation resulted in the retention of ICAM-1-targeted MB in the carotid artery. This was analyzed *ex vivo* both by US imaging and by microscopy, and findings were validated *in vivo*. With this approach, Wu and colleagues earlier already showed specific lesion-retention of ICAM-1-targeted MB, even under high (arterial) shear stress conditions, making this molecular US imaging approach potentially useful for differentiating between stable and vulnerable atherosclerotic plaques [48]. Similarly, Rix and colleagues recently tested $\alpha_v\beta_3$ integrin-targeted MB after vascular injury in pigs. In this study, employing MB modified with cyclic RGD peptide as a targeting moiety, it was found that $\alpha_v\beta_3$ integrin-targeted MB bind to endoarterial balloon injury sites, with a peak in integrin expression and MB binding after 1 week, and normalization back to baseline levels after 3 months [49].

The usefulness of antibody-targeted PBCA MB was also evaluated in neuroinflammation. ICAM-1 and VCAM-1 targeting was realized by coupling the respective biotinylated antibodies to streptavidin-coated MB. Contrast-enhanced US detected specific localization of these MB *in* vivo and *ex vivo* in the brain and spinal cord of rats with adoptive transfer

experimental autoimmune encephalomyelitis; responses to anti-inflammatory corticosteroid therapy could also be assessed, as the accumulation of ICAM-1-targeted MB decreased upon drug treatment [50, 51].

Together, these findings show that PBCA MB represent a versatile platform for molecular imaging of vascular injury and inflammation in angiology, addressing endothelial biomarkers such as VCAM-1, ICAM-1 and $\alpha_v\beta_3$ integrins.

3.3 PBCA MB for molecular imaging in oncology

Antibody- and peptide-targeted MB also hold potential for molecular US imaging in oncology (Figure 3C). To extend efforts in this direction, we coupled the IELLQAR peptide to the MB to target E-selectin, which is a marker for angiogenesis and which is known to be overexpressed during tumor progression. In A431 squamous cell carcinoma xenografts, these MB showed specific accumulation: when comparing pre- and post-MB US images, clear enhancements in signal intensity were observed (Figure 3D). The difference in signal intensity represents MB bound to the vascular wall, and is a measure for angiogenic marker expression. These findings in A431 tumors confirm previously published findings with E-selectin-targeted MB in MLS human ovarian cancer xenografts [46]. Spivak et al. used the same E-selectin-targeted MB to assess the impact of MB dosing. A dose of 7 x 10^7 MB per kg body weight was found to be sufficient to detect E-selectin expression in tumors and to monitor the effect of antiangiogenic therapy [52].

Another prominent target for molecular US imaging in oncology is VEGFR-2. Fokong and colleagues developed VEGFR-2-targeted PBCA MB by biotin/streptavidin-based antibody coupling, and showed specific accumulation and molecular US imaging in subcutaneous CT26 colon carcinoma xenografts in mice [53]. Along the same line of thinking, Palmowski et al. used VEGFR-2-targeted PBCA MB, and also $\alpha_v\beta_3$ integrin- and ICAM-1-targeted MB, for specific CEUS imaging and for the evaluation of changes in angiogenic biomarkers during anti-matrix-metalloproteinase therapy [54]. Moreover, in a syngeneic rat prostate carcinoma model, they observed specific accumulation of ICAM-1- and $\alpha_v\beta_3$-integrin-targeted MB, and an increase in both biomarkers upon heavy-ion radiotherapy (as opposed to a decrease in vessel density and vascular perfusion; which was found using functional US imaging) [55].

These preclinical examples illustrate the utility of targeted PBCA MB for molecular imaging and treatment monitoring of tumors. Relevant endothelial markers like VEGFR-2, E-selectin, ICAM-1, VCAM-1 and $\alpha_v\beta_3$-integrin can be specifically addressed via modifying the surface of PBCA MB with antibodies and peptides. The clinical evaluation of such targeted US contrast agents has recently been initiated, albeit with phospholipid-based MB, looking e.g. at the expression levels of VEGFR-2 in prostate cancer patients [56, 57].

3.4 PBCA MB for indirect drug delivery

Indirect drug delivery refers to sonoporation, which can assist in the permeation of endothelial linings and/or cell membranes. We analyzed the accumulation of the 70 kDa (10 nm) macromolecular model drug FITC-dextran in brain tissue after co-injection with PBCA MB and US treatment, and compared it with the accumulation and penetration of FITC-

dextran in non-sonicated controls (Figure 4A-B). Fluorescence microscopy showed high accumulation of the FITC-dextran around blood vessels in the brains of mice receiving MB and US treatment. No signal of extravasated FITC-dextran was visible in the brains of mice which were injected with MB but not treated by US, exemplifying successful indirect drug delivery across the BBB and to the brain upon sonoporation [58].

We mirrored these experiments in solid tumors, looking at the accumulation and penetration of 100 nm-sized fluorophore-labeled PEGylated liposomes in tumor models with low baseline levels of enhanced permeability and retention (EPR), i.e. highly cellularly dense A431 epidermoid xenografts and highly stromal BxPC3 pancreatic xenografts [59]. We compared PBCA-based polymeric MB to phospholipid-based MB, but did not observe obvious differences. It is worth mentioning, however, that the sonoporation protocols (dosing of MB and US, US setting, timing, etc.) have not yet been optimized to allow for accurate/detailed assessment of differences in sonoporation potential. Another interesting question is whether vascular targeting (e.g. using antibodies or peptides targeted to VEGFR-2 or E-selectin) enhances the efficacy of sonoporation. As sonoporation potential likely directly depends on the distance of oscillating/destroyed MB to the endothelial lining, targeting may allow for more efficient (and safe; in case of the brain) sonoporation. Finally, it has to be mentioned in this context that MB- and US-mediated indirect drug delivery has recently been performed in patients, albeit with phospholipid-based MB. These pioneering studies have shown that prolonged survival times can be obtained in pancreatic cancer patients treated with gemcitabine upon combining it with sonoporation [38, 56, 57]. A first trial in glioblastoma patients, treated with doxorubicin in combination with sonoporation has also recently started, and the outcomes of this study are eagerly awaited [39].

Together, these efforts exemplify the potential of combining MB with US to induce sonoporation of blood vessels at pathological sites, promoting the targeted delivery of drugs and drug delivery systems to tumors and to the brain

3.5 PBCA MB for direct drug delivery

Direct drug delivery refers to the use of MB containing drug molecules within their shell, and to their temporally and spatially controlled release upon exposure to US (Figure 4C). To provide initial proof-of-principle for direct drug delivery using PBCA-based MB, the fluorophores coumarin 6 (as a hydrophobic model drug) and rhodamine B (as a hydrophilic model drug) were encapsulated into the MB shell [53]. These MB were targeted to VEGFR-2 and their target-specific accumulation was confirmed in subcutaneous CT26 colon carcinoma tumors. For the evaluation of direct (model) drug delivery to tumors, 2D fluorescence microscopy was employed. As hypothesized, and as shown in Figure 4D (upper panel), the US-mediated destruction of PBCA MB in tumors resulted in efficient accumulation and penetration of the hydrophobic model drug coumarin 6. No accumulation was observed in control tumors, which were not exposed to US (lower panel).

In a similar setup, Wheatley and colleagues used polylactic acid (PLA) -based MB for direct drug delivery of doxorubicin and paclitaxel to tumors. In the VX2 liver tumor model in New Zealand rabbits, non-targeted doxorubicin-loaded PLA MB were locally destroyed by US at the tumorous site during circulation. ^{14}C-labeling of doxorubicin enabled assessment of the

target site accumulation of the drug. In comparison to non-sonicated tumors, significantly enhanced levels of doxorubicin were found in tumor tissue [60]. Extending these findings, in the Morris rat hepatocellular carcinoma model, doxorubicin-loaded MB induced tumor growth inhibition upon US-mediated MB destruction at the pathological site [61]. PLA MB loaded with paclitaxel have also been developed and employed. In *in vitro* model systems, based on the human breast cancer cell lines MDA-MB-231 and MCF7, these MB induced significantly more cell death when combined with US then when no US was applied [62].

In an alternative approach for MB-mediated direct drug delivery, pioneered (and patented) by scientists at SINTEF in Norway, the polymeric MB shell is composed of model drug-loaded PBCA nanoparticles (NP). Upon sonication, these MB disintegrate into 100-200 nm-sized nanoparticles, which can be deposited across sonoporated endothelium. Using these PBCA NP-stabilized MB, temporally and spatially controlled disruption of the BBB has already been demonstrated, as exemplified by the detection of Nile Red-loaded PBCA NP in the brain, as well as by the accumulation of the co-injected gadolinium-based MRI contrast agent Omniscan® in sonicated regions [62]. Using the same setup, PBCA NP delivery to and into prostate adenocarcinoma xenografts upon US exposure has also already been demonstrated, as evidence by fluorescence microscopy detection [64].

These findings show that that PBCA-based polymeric MB hold potential for direct drug delivery to tumors and to the brain, with drug molecules either embedded into the MB shell, or into NP constituting the MB shell, allowing for US-controlled delivery to pathological sites.

4 Conclusion

We demonstrate the broad applicability of PBCA-based polymeric MB for molecular imaging and drug delivery. Evidence is provided showing that (model) drug molecules can be efficiently loaded into the shell of PBCA MB. In addition, VCAM-1-targeting of inflamed blood vessels is shown in *ex vivo* flow chambers, and the feasibility of E-selectin-specific MB imaging of tumor angiogenesis is confirmed in A431 tumors. Furthermore, MB- and US-mediated sonoporation is demonstrated to result in BBB opening and in the accumulation of the macromolecular model drug FITC-dextran in the brain. Finally, we show that shell-incorporated model drugs can be efficiently shuttled across the vascular wall in CT26 tumors. These results exemplify the usefulness of PBCA MB for molecular US imaging of atherosclerosis and tumor angiogenesis. They also indicate that sonoporation-enhanced direct and indirect drug delivery to tumors and to the brain may contribute to more efficient disease treatment. Together, the findings summarized in this study illustrate that the potential and the broad applicability of PBCA-based polymeric MB.

Europe PMC Funders Author Manuscripts

Acknowledgements

The authors gratefully acknowledge financial support by the German Research Foundation (DFG: LA 2937/1-2), by the European Research Council (ERC-StG-309495-NeoNaNo), and by the i³tm Seed Fund Program (which is part of the Excellence Initiative of the German federal and State Governments; SF_14-4-09-Sonoporation). The authors also gratefully acknowledge input from the IZKF multiphoton imaging facility at RWTH Aachen University Clinic for assistance with the TPLSM experiments (Dr. Michael Vogt).

Europe PMC Funders Author Manuscripts

References

[1]. Wells PNT. Ultrasound imaging. Phys Med Biol. 2006; 51(13):83.

[2]. Bauer A, et al. Wideband harmonic imaging: A novel contrast ultrasound imaging technique. Eur Radiol. 1999; 9(3):364–367.

[3]. Tiemann K, et al. Stimulated acoustic emission: pseudo-Doppler shifts seen during the destruction of nonmoving microbubbles. Ultrasound in Medicine & Biology. 2000; 26(7):1161–1167. [PubMed: 11053751]

[4]. Cosgrove D. Future Prospects for SonoVue and CPS. Eur Radiol. 2004; 14(Suppl 8):116–124.

[5]. Ehling J, Lammers T, Kiessling F. Non-Invasive Imaging for Studying Anti-Angiogenic Therapy Effects. Thromb Haemost. 2013; 109(3):375–390. [PubMed: 23407722]

[6]. Strobel D, et al. Tumor-Specific Vascularization Pattern of Liver Metastasis, Hepatocellular Carcinoma, Hemangioma and Focal Nodular Hyperplasia in the Differential Diagnosis of 1349 Liver Lesions in Contrast-Enhanced Ultrasound (CEUS). Ultraschall in der Medizin - European Journal of Ultrasound. 2009; 30(04):376–382. [PubMed: 19688669]

[7]. Mulvagh SL, et al. American Society of Echocardiography Consensus Statement on the Clinical Applications of Ultrasonic Contrast Agents in Echocardiography. Journal of the American Society of Echocardiography. 2008; 21(11):1179–1201. [PubMed: 18992671]

[8]. P M, et al. Vessel fractions in tumor xenografts depicted by flow- or contrast-sensitive three-dimensional high-frequency Doppler ultrasound respond differently to antiangiogenic treatment. Cancer Res. 2008; 68(17):7042–7049. [PubMed: 18757418]

[9]. Baetke SC, et al. Squamous Cell Carcinoma Xenografts: Use of VEGFR2-targeted Microbubbles for Combined Functional and Molecular US to Monitor Antiangiogenic Therapy Effects. Radiology. 2015; 278(2):430–440. [PubMed: 26313618]

[10]. Hanahan D, Weinberg RA. Hallmarks of Cancer: The Next Generation. Cell. 2011; 144(5):646–674. [PubMed: 21376230]

[11]. Kiessling F, Fokong S, Bzyl J, Lederle W, Palmowski M, Lammers T. Recent advances in molecular, multimodal and theranostic ultrasound imaging. Advanced Drug Delivery Reviews. 2014; 72:15–27. [PubMed: 24316070]

[12]. Hicklin DJ, Ellis LM. Role of the Vascular Endothelial Growth Factor Pathway in Tumor Growth and Angiogenesis. JCO. 2005; 23(5):1011–1027.

[13]. Libby P, Ridker PM, Maseri A. Inflammation and atherosclerosis. Circulation. 2002; 105(9): 1135–1143. [PubMed: 11877368]

[14]. Hood JD, Cheresh DA. Role of integrins in cell invasion and migration. Nat Rev Cancer. 2002; 2(2):91–100. [PubMed: 12635172]

[15]. Grivennikov SI, Greten FR, Karin M. Immunity, Inflammation, and Cancer. Cell. 2010; 140(6): 883–899. [PubMed: 20303878]

[16]. Lindner JR, Song J, Christiansen J, Klibanov AL, Xu F, Ley K. Ultrasound Assessment of Inflammation and Renal Tissue Injury With Microbubbles Targeted to P-Selectin. Circulation. 2001; 104(17):2107–2112. [PubMed: 11673354]

[17]. Karshafian RR, Bevan PD, Williams R, Samac S, Burns PN. Sonoporation by Ultrasound-Activated Microbubble Contrast Agents: Effect of Acoustic Exposure Parameters on Cell Membrane Permeability and Cell Viability. Ultrasound in Medicine & Biology. 2009; 35(5):847–860. [PubMed: 19110370]

[18]. Tran TA, Guennec JYL, Bougnoux P, Tranquart F, Bouakaz A. Characterization of cell membrane response to ultrasound activated microbubbles. IEEE Transactions on Ultrasonics, Ferroelectrics, and Frequency Control. 2008; 55(1):43–49.

[19]. Derieppe M, Rojek K, Escoffre J-M, de Senneville BD, Moonen C, Bos C. Recruitment of endocytosis in sonopermeabilization-mediated drug delivery: a real-time study. Phys Biol. 2015; 12(4):046010. [PubMed: 26118644]

[20]. van Wamel A, et al. Vibrating microbubbles poking individual cells: Drug transfer into cells via sonoporation. Journal of Controlled Release. 2006; 112(2):149–155. [PubMed: 16556469]

[21]. Unger EC, Hersh E, Vannan M, Matsunaga TO, McCreery T. Local drug and gene delivery through microbubbles. Progress in Cardiovascular Diseases. 2001; 44(1):45–54. [PubMed: 11533926]

[22]. Liu Y, Miyoshi H, Nakamura M. Encapsulated ultrasound microbubbles: Therapeutic application in drug/gene delivery. Journal of Controlled Release. 2006; 114(1):89–99. [PubMed: 16824637]

[23]. Lentacker I, Smedt SCD, Sanders NN. Drug loaded microbubble design for ultrasound triggered delivery. Soft Matter. 2009; 5(11):2161–2170.

[24]. Ting C-Y, et al. Concurrent blood–brain barrier opening and local drug delivery using drug-carrying microbubbles and focused ultrasound for brain glioma treatment. Biomaterials. 2012; 33(2):704–712. [PubMed: 22019122]

[25]. Liu H-L, Fan C-H, Ting C-Y, Yeh C-K. Combining Microbubbles and Ultrasound for Drug Delivery to Brain Tumors: Current Progress and Overview. Theranostics. 2014; 4(4):432–444. [PubMed: 24578726]

[26]. Lindner JR. Microbubbles in medical imaging: current applications and future directions. Nat Rev Drug Discov. 2004; 3(6):527–533. [PubMed: 15173842]

[27]. Kiessling F, Fokong S, Koczera P, Lederle W, Lammers T. Ultrasound Microbubbles for Molecular Diagnosis, Therapy, and Theranostics. J Nucl Med. 2012; 53(3):345–348. [PubMed: 22393225]

[28]. Lentacker I, De Cock I, Deckers R, De Smedt SC, Moonen CTW. Understanding ultrasound induced sonoporation: Definitions and underlying mechanisms. Advanced Drug Delivery Reviews. 2014; 72:49–64. [PubMed: 24270006]

[29]. Dasgupta A, Liu M, Ojha T, Storm G, Kiessling F, Lammers T. Ultrasound-mediated drug delivery to the brain: principles, progress and prospects. Drug Discovery Today: Technologies. 2016; 20:41–48. [PubMed: 27986222]

[30]. Lammertink BHA, Bos C, Deckers R, Storm G, Moonen CTW, Escoffre J-M. Sonochemotherapy: from bench to bedside. Front Pharmacol. 2015; 6:138. [PubMed: 26217226]

[31]. Böhmer MR, Chlon CHT, Raju BI, Chin CT, Shevchenko T, Klibanov AL. Focused ultrasound and microbubbles for enhanced extravasation. Journal of Controlled Release. 2010; 148(1):18–24. [PubMed: 20600402]

[32]. Yang F-Y, Lin Y-S, Kang K-H, Chao T-K. Reversible blood–brain barrier disruption by repeated transcranial focused ultrasound allows enhanced extravasation. Journal of Controlled Release. 2011; 150(1):111–116. [PubMed: 21070825]

[33]. Lammers T, Kiessling F, Hennink WE, Storm G. Drug targeting to tumors: Principles, pitfalls and (pre-) clinical progress. Journal of Controlled Release. 2012; 161(2):175–187. [PubMed: 21945285]

[34]. Ernsting, MJ., Worthington, A., May, JP., Tagami, T., Kolios, MC., Li, SD. Ultrasound drug targeting to tumors with thermosensitive liposomes. IEEE International Ultrasonics Symposium; 2011. p. 1-4.

[35]. Staruch RM, Ganguly M, Tannock IF, Hynynen K, Chopra R. Enhanced drug delivery in rabbit VX2 tumours using thermosensitive liposomes and MRI-controlled focused ultrasound hyperthermia. International Journal of Hyperthermia. 2012; 28(8):776–787. [PubMed: 23153219]

[36]. Kheirolomoom A, et al. Complete regression of local cancer using temperature-sensitive liposomes combined with ultrasound-mediated hyperthermia. Journal of Controlled Release. 2013; 172(1):266–273. [PubMed: 23994755]

[37]. [accessed January 12, 2017] Targeted Chemotherapy Using Focused Ultrasound for Liver Tumours (TARDOX). ClinicalTrials.Gov. (n.d.). https://clinicaltrials.gov/ct2/show/study/NCT02181075?term=Thermodox&rank=5

[38]. Dimcevski G, et al. A human clinical trial using ultrasound and microbubbles to enhance gemcitabine treatment of inoperable pancreatic cancer. Journal of Controlled Release. 2016; 243:172–181. [PubMed: 27744037]

[39]. [accessed January 12, 2017] Blood-Brain Barrier Disruption Using Transcranial MRI-Guided Focused Ultrasound. ClinicalTrials.Gov. (n.d.). https://clinicaltrials.gov/ct2/show/study/NCT02343991?term=NCT02343991&rank=1

[40]. Cavalieri F, Zhou M, Tortora M, Lucilla B, Ashokkumar M. Methods of Preparation of Multifunctional Microbubbles and their In Vitro / In Vivo Assessment of Stability, Functional and Structural Properties. Current Pharmaceutical Design. 2012; 18(15):2135–2151. [PubMed: 22352769]

[41]. Sirsi SR, Borden MA. Microbubble compositions, properties and biomedical applications. Bubble Science, Engineering & Technology. 2009; 1(1–2):3–17. [PubMed: 20574549]

[42]. Koczera P, et al. Fluorescently labeled microbubbles for facilitating translational molecular ultrasound studies. Drug Deliv and Transl Res. 2012; 2(1):56–64. [PubMed: 25786599]

[43]. Joseph S, Olbrich C, Kirsch J, Hasbach M, Briel A, Schirner M. A Real-Time in Vitro Assay for Studying Functional Characteristics of Target-Specific Ultrasound Contrast Agents. Pharm Res. 2004; 21(6):920–926. [PubMed: 15212154]

[44]. Palmowski M, et al. Pharmacodynamics of streptavidin-coated cyanoacrylate microbubbles designed for molecular ultrasound imaging. Invest Radiol. 2008; 43(3):162–169. [PubMed: 18301312]

[45]. Olbrich C, et al. The in vitro stability of air-filled polybutylcyanoacrylate microparticles. Biomaterials. 2006; 27(19):3549–3559. [PubMed: 16537092]

[46]. Fokong S, et al. Ultrasound Molecular Imaging of E-Selectin in Tumor Vessels Using Poly n-Butyl Cyanoacrylate Microbubbles Covalently Coupled to a Short Targeting Peptide. Investigative Radiology. 2013; 48(12):843–850. [PubMed: 23857137]

[47]. Curaj A, et al. Noninvasive Molecular Ultrasound Monitoring of Vessel Healing After Intravascular Surgical Procedures in a Preclinical Setup. Arterioscler Thromb Vasc Biol. 2015; 35(6):1366–1373. [PubMed: 25838431]

[48]. Wu Z, et al. Rhodamine-loaded intercellular adhesion molecule-1-targeted microbubbles for dual-modality imaging under controlled shear stresses. Circ Cardiovasc Imaging. 2013; 6(6):974–981. [PubMed: 24036383]

[49]. Rix A, et al. Molecular Ultrasound Imaging of $\alpha_V\beta_3$-Integrin Expression in Carotid Arteries of Pigs After Vessel Injury. Invest Radiol. 2016; 51(12):767–775. [PubMed: 27119438]

[50]. Linker RA, et al. In vivo molecular imaging of adhesion molecules in experimental autoimmune encephalomyelitis (EAE). Journal of Autoimmunity. 2005; 25(3):199–205. [PubMed: 16249069]

[51]. Reinhardt M, et al. Ultrasound derived imaging and quantification of cell adhesion molecules in experimental autoimmune encephalomyelitis (EAE) by Sensitive Particle Acoustic Quantification (SPAQ). NeuroImage. 2005; 27(2):267–278. [PubMed: 15905104]

[52]. Spivak I, et al. Low-Dose Molecular Ultrasound Imaging with E-Selectin-Targeted PBCA Microbubbles. Mol Imaging Biol. 2016; 18(2):180–190. [PubMed: 26391990]

[53]. Fokong S, et al. Image-guided, targeted and triggered drug delivery to tumors using polymer-based microbubbles. Journal of Controlled Release. 2012; 163(1):75–81. [PubMed: 22580225]

[54]. Palmowski M, et al. Molecular profiling of angiogenesis with targeted ultrasound imaging: early assessment of antiangiogenic therapy effects. Mol Cancer Ther. 2008; 7(1):101–109. [PubMed: 18202013]

[55]. Palmowski M, et al. Molecular Ultrasound Imaging of Early Vascular Response in Prostate Tumors Irradiated with Carbon Ions. Neoplasia. 2009; 11(9):856–863. [PubMed: 19724679]

[56]. [accessed January 12, 2017] BR55 in Prostate Cancer: an Exploratory Clinical Trial, BR55 in Prostate Cancer: an Exploratory Clinical Trial. ClinicalTrials.Gov. (n.d.) https://clinicaltrials.gov/ct2/show/NCT01253213

[57]. [accessed January 12, 2017] A Pilot Trial Using BR55 Ultrasound Contrast Agent in the Assessment of Prostate Cancer. ClinicalTrials.Gov. (n.d.) https://clinicaltrials.gov/ct2/show/NCT02142608?term=NCT02142608&rank=1

[58]. Lammers T, et al. Theranostic USPIO-Loaded Microbubbles for Mediating and Monitoring Blood-Brain Barrier Permeation. Adv Funct Mater. 2015; 25(1):36–43. [PubMed: 25729344]

[59]. Theek B, et al. Sonoporation enhances liposome accumulation and penetration in tumors with low EPR. Journal of Controlled Release. 2016; 231:77–85. [PubMed: 26878973]

[60]. Eisenbrey JR, Soulen MC, Wheatley MA. Delivery of Encapsulated Doxorubicin by Ultrasound-Mediated Size Reduction of Drug-Loaded Polymer Contrast Agents. IEEE Transactions on Biomedical Engineering. 2010; 57(1):24–28. [PubMed: 19709952]

[61]. Cochran MC, et al. Disposition of Ultrasound Sensitive Polymeric Drug Carrier in a Rat Hepatocellular Carcinoma Model. Academic Radiology. 2011; 18(11):1341–1348. [PubMed: 21971256]

[62]. Cochran MC, Eisenbrey J, Ouma RO, Soulen M, Wheatley MA. Doxorubicin and paclitaxel loaded microbubbles for ultrasound triggered drug delivery. International Journal of Pharmaceutics. 2011; 414(1–2):161–170. [PubMed: 21609756]

[63]. Åslund AKO, et al. Nanoparticle delivery to the brain — By focused ultrasound and self-assembled nanoparticle-stabilized microbubbles. Journal of Controlled Release. 2015; 220(Part A):287–294. [PubMed: 26518721]

[64]. Eggen S, et al. Ultrasound-enhanced drug delivery in prostate cancer xenografts by nanoparticles stabilizing microbubbles. Journal of Controlled Release. 2014; 187:39–49. [PubMed: 24852099]

Europe PMC Funders Author Manuscripts

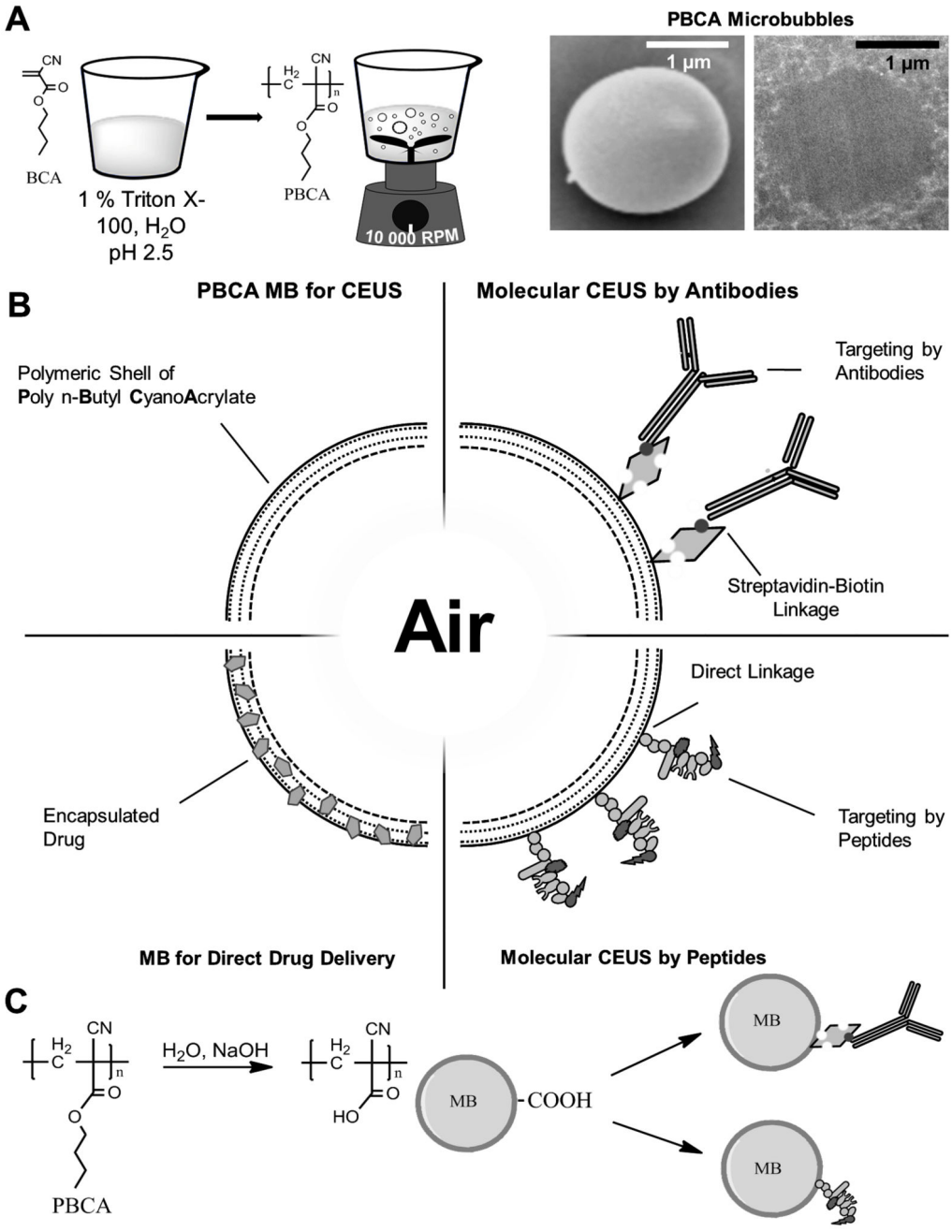

Figure 1. Synthesis and functionalization of PBCA-based polymeric MB.

A: BCA monomers are added to an aqueous solution containing the surfactant Triton X-100 at pH 2.5. Vigorous stirring creates polydisperse MB with PBCA as the shell material. Scanning (SEM) and transmission (TEM) electron microscopy exemplify the spherical shape of PBCA MB. B: Schematic depiction of the surface-functionalization and shell-loading of PBCA MB, making them useful for molecular imaging and drug delivery. Coupling of antibodies and peptides as targeting moieties for molecular imaging targeted drug delivery can be performed by biotin-streptavidin linkages, as well as via direct

chemical coupling mechanisms. C: For surface-functionalization, the shell of PBCA MB is hydrolyzed to create carboxyl-groups for chemical coupling to targeting ligands.

Europe PMC Funders Author Manuscripts

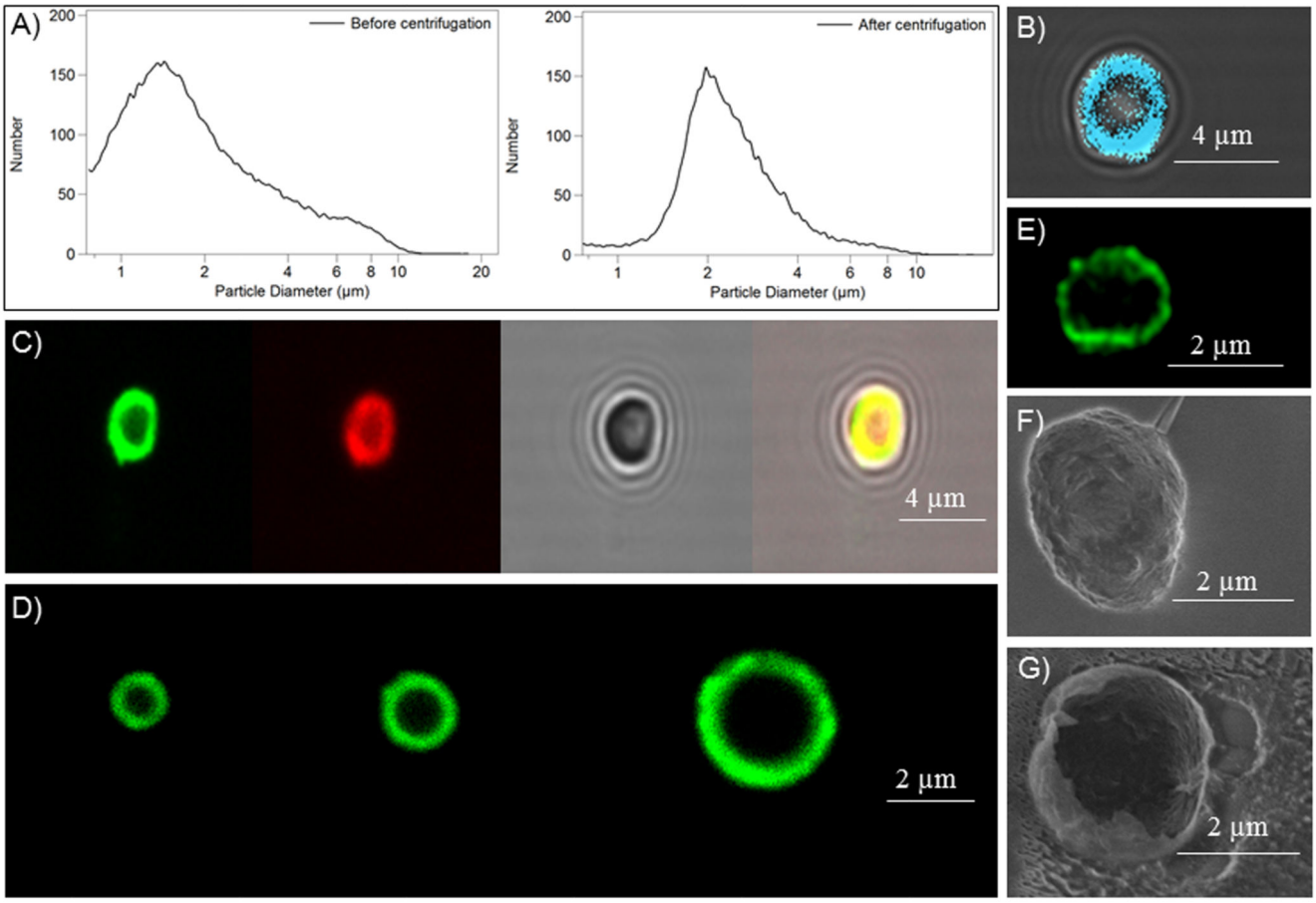

Figure 2. Characterization and loading of PBCA-based polymeric MB.

A: Size distribution of MB before and after centrifugation and flotation. B-D: Fluorescence microscopy images of HITC-loaded MB (B), individual and co-loading of rhodamine B and coumarin 6 into MB (C), and differently-sized MB batches loaded with coumarin 6 (D). E: STED microscopy image of a coumarin 6-loaded MB. F-G: Scanning electron microscopy (SEM) images of an intact (F) and a destroyed (G) PBCA MB.

Europe PMC Funders Author Manuscripts

Europe PMC Funders Author Manuscripts

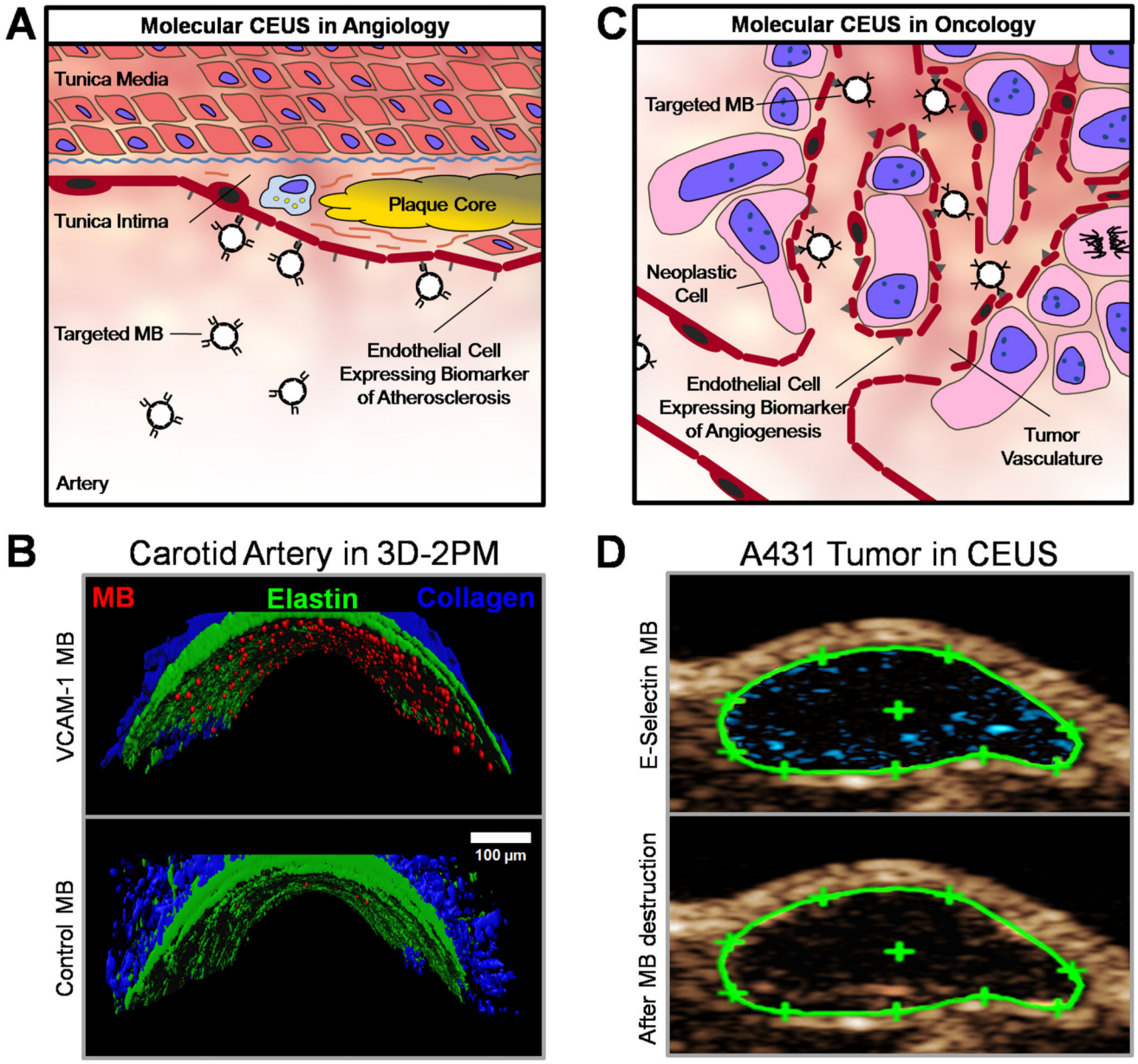

Figure 3. PBCA-based polymeric MB for molecular imaging.

A: Schematic depiction of the retention of ligand-targeted MB for contrast-enhanced US imaging of endothelial biomarkers in atherosclerosis. B: Ex vivo binding of rhodamine-labeled VCAM-1-targeted MB to an explanted murine carotid artery after TNF-α stimulation, as assessed by 3D two-photon laser scanning microscopy (3D-2PM). VCAM-1-targeted MB bind to activated endothelial cells and show retention under physiological shear stress (upper panel), whereas untargeted MB hardly associate with inflamed blood vessels (lower panel). Rhodamine-labeled MB are shown in red, elastin autofluorescence in green, and second harmonic generation imaging of collagen is depicted in blue. C: Illustration of the binding of targeted MB for contrast-enhanced US of angiogenesis biomarkers during

tumor progression. D: Non-linear molecular US imaging of peptide-modified MB recognizing E-selectin on tumor blood vessels in subcutaneous A431 xenograft tumors. Signal enhancement (in blue) as a difference of contrast intensity before (upper panel) and after (lower panel) MB destruction by destructive US pulses allows for the assessment of E-selectin expression, and analysis of tumor vascularization and angiogenesis.

Europe PMC Funders Author Manuscripts

Europe PMC Funders Author Manuscripts

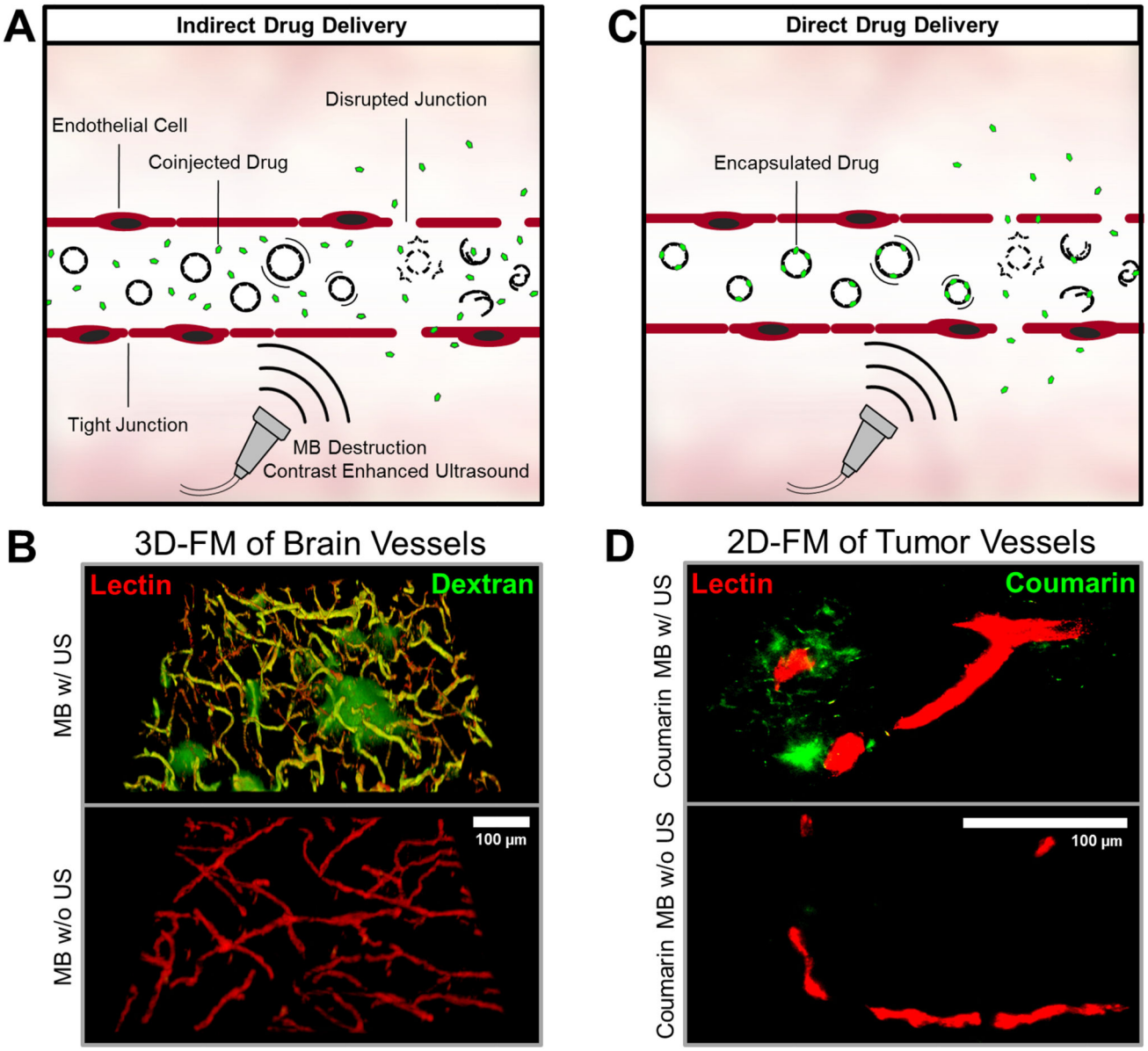

Figure 4. PBCA-based polymeric MB for indirect and direct drug delivery.

A+C: After i.v. injection, MB can be used to enhance the permeability and penetration of co-administered (A: indirect drug delivery) or co-formulated (B: direct drug delivery) drugs and drug delivery systems. B: Ex vivo two-photon laser scanning microscopy (3D-FM) of the extravasation of the macromolecular model drug FITC-dextran (green) across the blood-brain barrier. Rhodamine-lectin-stained blood vessels are shown red. Upon US-induced MB destruction (upper panel), the accumulation and penetration of FITC-dextran can be clearly detected in the mouse brain. No FITC-dextran extravasation is observed if US is omitted (lower panel). D: Ex vivo fluorescence microscopy (2D-FM) images of coumarin 6 (green) accumulation, released from the MB shell or entrapped within MB shell fragments, in subcutaneous CT26 colon carcinoma tumors in mice, in relation to rhodamine-lectin-stained

tumor blood vessels (red). Upon US-mediated MB destruction of VEGFR-2-targeted and coumarin 6-loaded MB, substantially enhanced model drug delivery to and into tumorous tissue can be observed.

Europe PMC Funders Author Manuscripts